Biomedical Signal Processing and Control 57 (2020) 101779

Contents lists available at ScienceDirect

Biomedical Signal Processing and Control

journal homepage: www.elsevier.com/locate/bspc

Estimation of heart rate and respiratory rate from the seismocardiogram under resting state

Yue-Der Lin [a,b,*], Ya-Fen Jhou [b,c]

[a] Department of Automatic Control Engineering, Feng Chia University, Taichung, Taiwan
[b] Master's Program of Biomedical Informatics and Biomedical Engineering, Feng Chia University, Taichung Taiwan
[c] ACME Portable Corp, New Taipei City, Taiwan

ARTICLE INFO

Article history:
Received 2 February 2019
Received in revised form 12 October 2019
Accepted 16 November 2019
Available online 9 December 2019

Keywords:
Agreement analysis
Envelogram
Heart rate (HR)
Intraclass correlation coefficient (ICC)
Respiratory rate (RR)
Scalogram
Seismocardiogram (SCG)
Wavelet decomposition

ABSTRACT

This study proposes a dedicated algorithm to estimate heart rate (HR) and respiratory rate (RR) from seismocardiogram (SCG). The proposed algorithm primarily consists of the wavelet decomposition (by db6 wavelet), the Fourier-based envelope detection and the time-averaged power spectral density (PSD) from the scalogram by complex Morlet wavelet. The records in the combined measurement of ECG, breathing and SCG (CEBS) database of PhysioNet are adopted to evaluate the performance of the proposed algorithm for HR and RR estimation. The performance was evaluated by intraclass correlation coefficient (ICC) and Bland-Altman's agreement analysis.

The statistical results for HR estimation show good to excellent correlation between the approaches by SCG and ECG and also meet the maximal allowable error for the HR meter. As the quality of some respiratory signals in the CEBS database is not good for RR estimation, additional experiments have been conducted in the university laboratory under well-controlled procedure. The statistical results for the RR estimation in these experiments show good to excellent correlation between the approaches of RR estimation by SCG and respiratory signal. The RR estimation from SCG also meets the specification given in contemporary medical device.

The proposed algorithm does not take the removal of motion artifact into account and thus SCG signal must be measured under resting state. From this study, SCG can be a potential tool to estimate HR and RR for monitoring the patient in intensive care unit (ICU) or monitoring the sleep quality in clinical setting or in daily life.

1. Introduction

In clinical setting, monitoring of resting heart rate (HR) has been verified to be crucial for the evaluation of mortality [1,2], the prediction of cardiovascular diseases [3] and the prognostic evaluation for coronary artery disease (CAD) [4]. Respiratory rate (RR) is another important vital sign widely adopted in clinical medicine. The value of RR has been used to identify the serious illness for inpatients [5,6] and is an indication of clinical deterioration after emergency department discharge or acute care [7,8]. The gold standard for continuous HR monitoring is from the measurement of electrocardiogram (ECG), whereas that for RR monitoring is the capnography, especially for the cases in anesthesia [9]. In general care settings, RR can also be measured by impedance plethysmography [10], multi-lead ECG [11], temperature variation in the breathing flow [12], triaxial accelerometer [13,14], acoustic sensor [15] and photoplethysmogram (PPG) [16,17]. Continuous monitoring of vital signs, especially HR and RR, can provide valuable information to the clinicians as an early warning of deterioration and clinical decision based on the clinical data for the hospitalized patients [18]. Continuous monitoring of HR and RR is also closely associated with the decrease of stay length in the hospital or in intensive care unit (ICU) for transferred patients [19]. Simultaneous monitoring of HR and RR usually needs two respective standard equipments, which would make the accessory lead wires and conduits of the used equipments cumbersome. It would be competitive and attractive to monitor more vital signs by a single device in practical applications. Among various approaches, ECG or PPG can be adopted to monitor HR and RR simultaneously by a single equipment [11,16,17].

Due to the technology advancement of microelectromechanical system (MEMS), the so-called seismocardiogram (SCG) measured from the chest of subject by miniature accelerometer can be acquired in much lower cost than ever. The accelerometer is a

* Corresponding author at: Department of Automatic Control Engineering, Feng Chia University, Taichung, Taiwan.
E-mail addresses: ydlin@fcu.edu.tw, yudlin@me.com (Y.-D. Lin).

https://doi.org/10.1016/j.bspc.2019.101779
1746-8094/

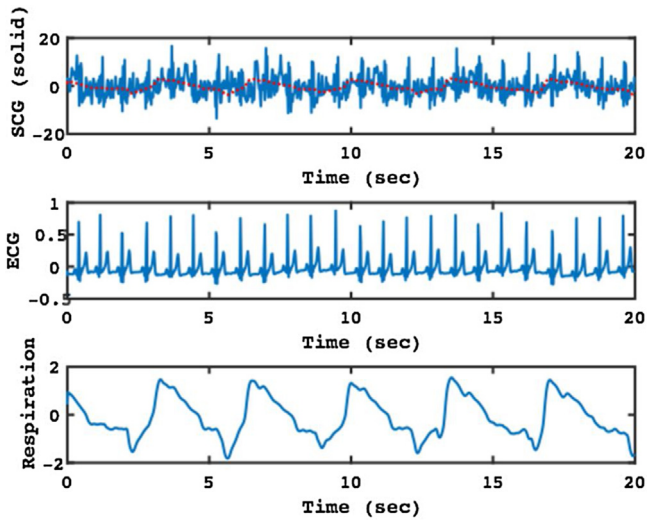

Fig. 1. Time-domain patterns of twenty-second length recorded simultaneously for SCG, ECG and respiratory signal from the data numbered b017. Top: SCG (solid line) with the corresponding respiratory signal (dotted line) shown for convenient comparison; middle: ECG; bottom: respiratory signal.

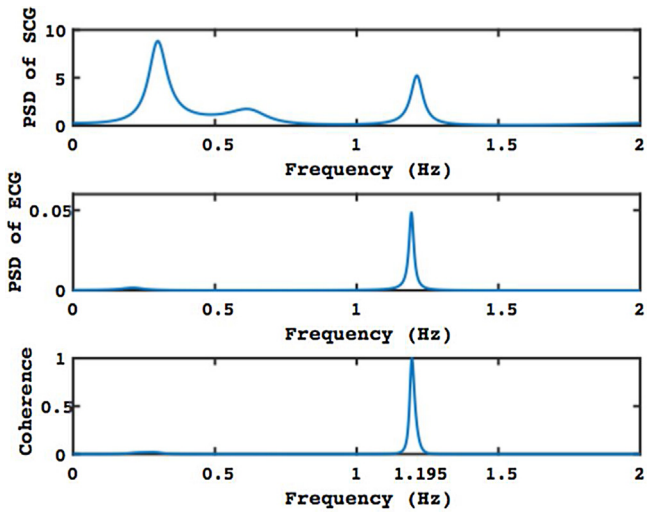

Fig. 2. The power spectral density (PSD) for SCG and ECG, and their coherence for the data numbered b017. Top: PSD of SCG; middle: PSD of ECG; bottom: the coherence between the PSD of SCG and ECG.

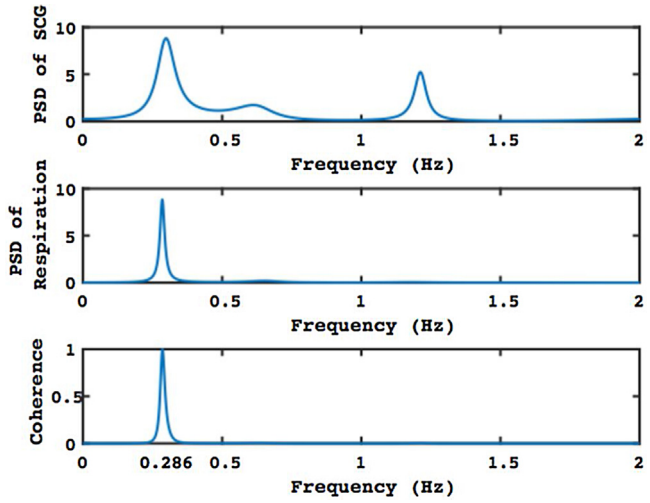

Fig. 3. The PSD for SCG and respiratory signal, and their coherence for the data numbered b017. Top: PSD of SCG; middle: PSD of respiratory signal; bottom: the coherence between the PSD of SCG and respiratory signal.

device that reflects the external acceleration and is generally manufactured by the MEMS technology to satisfy the requirements of linearity, high sensitivity, multiple axes, large dynamic range, large bandwidth, and so on. This device possesses a number of sensing elements that are attached to the proof mass, which is suspended in a manner that allows it to move relative to the substrate. From Newton's second law of motion, an external acceleration will produce the displacement of proof mass. The displaced proof mass will lead to a change on some physical quantity such as the capacitance between the proof mass and the substrate. The sensing element is dedicated to linearly reflecting the quantity change in analog or digital form, generally in the unit of volt [20]. Fig. 1 demonstrates an example of SCG (top, solid line) with simultaneous ECG (middle, lead II) and respiratory signal (bottom) which is adopted from a twenty-second segment of number b017 in the combined measurement of ECG, breathing, and SCG (CEBS) database [21,22] of PhysioNet [23]. The top subfigure of Fig. 1 also shows the respiratory signal (in dotted line), and it can be observed that the respiratory component is also buried in the content of SCG. In addition, the timing of QRS complex in lead-II ECG also agrees well with the timing of the spikes in SCG as looking at the patterns shown in the top and middle subfigures. The components contained in SCG, ECG and respiratory signal can be recognized more easily in frequency domain. Fig. 2 demonstrates the power spectral density (PSD) of SCG (top), PSD of ECG (middle) and the coherence between the PSD of SCG and ECG (bottom) for the respective time-domain patterns shown in Fig. 1. High coherence at 1.195 Hz depicts that both SCG and ECG contain the same frequency component. Fig. 3 shows the PSD of SCG (top), PSD of respiratory signal (middle) and the coherence between the PSD of SCG and respiratory signal (bottom) for the corresponding time-domain patterns shown in Fig. 1. It can be observed that there is a high coherence occurred at 0.286 Hz in the bottom subfigure of Fig. 3 and this shows the same frequency component existed in both SCG and respiratory signal. In both Figs. 2 and 3, autoregressive (AR) PSD by Burg's method [24] is adopted for the spectral estimation with an order of 10 and a frequency resolution of 0.001 Hz. The results shown in Figs. 2 and 3 also represent that it is highly potential for the simultaneous monitoring of HR and RR by SCG. Compared with the measurement of ECG or PPG, SCG possesses the advantages of lower sensor cost and relatively less complicated measuring procedure. For these reasons, SCG has been adopted in many researches. For example, Drummond et al. utilized an encapsulated triaxial accelerometer to monitor the respiratory movements and estimate RR in clinical environment [13]. Pandia et al. developed specific algorithms to extract the respiration-related features (including RR) from SCG [14]. García-González et al. verified that SCG can be used instead of ECG to obtain the reliable beat-to-beat interval sequence in the quiet condition [21]. Jafari Tadi et al. presented an adaptive beat identification technique based on Hilbert transform to detect the heartbeat timings from SCG for healthy volunteers in three different postures, and the acquired beat-to-beat interval sequences agree well with those from ECG [25]. In addition to the monitoring of heartbeat or respiration, SCG has also been applied in detection of coronary ischemia [26], diagnosis of coronary artery disease [27], identification of cardiac quiescence for cardiac imaging [28], detection of myocardial ischemia [29], estimation of pulse transit time [30], heart sound monitoring [31], detection of atrial fibrillation [32], identification of location-related features in the cardiac cycle [33], and so on. The plentiful research on SCG demonstrates its potential in clinical applications.

As shown in Figs. 2 and 3, the estimation of HR and RR may be obtained by the spectrum analysis of SCG signal. Among various approaches, AR PSD is an attractive choice because it has the advantages of shorter signal length needed in computation and finer frequency resolution compared with the Fourier-based methods. However, the method of AR PSD must satisfy several basic requirements such as high signal-to-noise ratio (SNR) [34] and proper selection on the model order [35]. For the problem of HR and RR estimation from SCG, the SCG signal can be considered to be composed of the components from heartbeat, respiration and the body motion. In addition, the signal quality also depends upon the measurement position and the sensor attachment style. Therefore, SCG signal usually needs to be de-noised before further processing such as spectrum analysis. Because the frequencies of heartbeat and respiration are variable, the cutoff frequencies for bandpass filters are not easily determined in such case. For this condition, wavelet analysis is a feasible choice for de-noising. This approach has been widely adopted in many biomedical applications [36]. In addition, reference [21] utilized the method of wavelet decomposition for filtered SCG to detect the heartbeat information and derived the standard deviation of error smaller than 3 ms. Pouymiro et al. also applied the wavelet decomposition to detect the fiducial points associated with the opening of aortic valve and isovolumic moment from SCG without the use of ECG for timing reference [37]. Based on the researches mentioned previously, this study also utilized the approach of wavelet decomposition to the de-noising of SCG.

The principal objective of this study is to verify the feasibility of HR and RR estimation by SCG signal. Previous researches primarily devote to acquiring either the normal heartbeat detection [21] or the RR estimation [13,14] from SCG. To date, no research has been dedicated to estimating HR and RR simultaneously from SCG. This paper is the first one to demonstrate how to acquire HR and RR simultaneously from SCG signal. This paper proposes a dedicated estimation algorithm which primarily utilizes the wavelet decomposition of SCG and the values of HR and RR are estimated from the derived scalograms. The computational complexity of the proposed algorithm is low enough to be executed in the embedded system. In addition to using the CEBS database, this study has also implemented the SCG sensor system and conducted physiological experiments to collect high-quality signals under resting state. The obtained signals are utilized to verify the correctness of RR estimation. The estimations by SCG in this research are compared with those derived by the respective gold standard approach and are tested by intraclass correlation coefficient (ICC) [38,39] and Bland-Altman agreement analysis [40]. The rigorous statistical tests make the analysis results credible. The detailed description will be introduced in later sections. The remainder of this paper is organized as follows. The proposed algorithm and the experiments conducted in this study are presented in Section 2. The experimental results and the respective discussion are shown in Section 3. Section 4 is the conclusion for this paper.

2. Method and materials

In this section, the proposed algorithm for HR and RR estimation in this study are stated in the first subsection. The second subsection describes the adopted database for HR and RR estimation and the conducted experiments for verification of RR estimation. The equipment and software adopted in this study are also presented in this subsection. The last subsection introduces the adopted statistical analysis methods.

In this study, the proposed algorithm and the statistical analysis were implemented and performed in MATLAB (2018a, MathWorks®, Inc., USA). All of the computations, including the statistical analysis, were executed on MacBook Pro (2.5 GHz Intel Core i7, with 16 GB memory size, Apple, Inc., USA).

2.1. Proposed algorithm

The algorithm includes three parts. The first part is the utilization of wavelet for the decomposition of SCG signal to extract the components related to heartbeat and respiration. The second one is the so-called envelogram which is used for the decomposed SCG signal that is related to heartbeat component. The purpose of envelogram is to make the shape of extracted heartbeat component similar to that of ECG signal such that the computation of heartbeat frequency could be more precise. The last part is the scalogram by complex Morlet wavelet which is used to derive the frequencies of heartbeat and respiration and the values of HR and RR could then be computed.

2.1.1. Wavelet decomposition

In this study, dyadic tree-structured wavelet decomposition is conducted to extract the information related to heartbeat and respiration from SCG signal. Among miscellaneous types of wavelets, the Daubechies wavelet is selected for the sake of its potential in the implementation of fast algorithm. Daubechies wavelets are a family of orthogonal wavelets characterized by the maximal number of vanishing moments for given support and have been widely used for various applications in signal analysis [42]. In this paper, Daubechies 6 wavelet (db6) is adopted for the reason of the moderately smooth shape on wavelet function. Another reason is that the oscillating pattern of db6 wavelet is similar to the shape of heartbeat and respiration pattern buried in SCG under different scales. In dyadic tree-structured wavelet decomposition, the signal is firstly split into low- and high-frequency components in the first level. The low-frequency subband provides the coarser part in the original signal, whereas the high-frequency subband contains the detailed information of the original signal, and they are respectively termed as the approximation and the detail in wavelet analysis. This first low-frequency subband component is then downsampled by a factor of 2 and again decomposed into low- and high-frequency subbands. The primary purpose of downsampling by a factor 2 is to make the data length unchanged before and after the decomposition process and this implies the computation results could be saved in the same memory space. This process can be continued to J levels as desired. The sequence after downsampling for the approximation is named as the approximate coefficients and that for the detail is termed as the detail coefficients [41]. At level j, let's denote them by $cA(j,k)$ and $cD(j,k)$ respectively, with k belonging to a positive integer. If the length of the original signal is N, the range of k at the level j is $1 \le k \le N/2^j$.

Let $s(n)$ denote the discrete-time signal at time index n, with $1 \le n \le N$. The signal $s(n)$ is decomposed by wavelet function to J levels, and assume that the approximate coefficients $cA(J, k)$ and the detail coefficients $cD(j, k)$ are acquired for $1 \le j \le J$ and k is a positive integer. The relationship between signal energy and wavelet coefficients can then be expressed as

$$\sum_{n=1}^{N}\left|s(n)\right|^2 = \sum_{k=1}^{N/2^J}\left|cA(J,k)\right|^2 + \sum_{j=1}^{J}\sum_{k=1}^{N/2^j}\left|cD(j,k)\right|^2. \quad (1)$$

With the downsampling being omitted in the whole decomposition process, let the detail and the approximation at level j be denoted by $Dj(\cdot)$ and $Aj(\cdot)$ respectively. If the signal $s(n)$ is decomposed by wavelet function with the J-level dyadic tree-structured procedure, then we have [43]

$$s(\cdot) = AJ(\cdot) + \sum_{j=1}^{J} Dj(\cdot). \quad (2)$$

Table 1
Wavelet decomposition levels and the corresponding frequency range.

Decomposed Component	Frequency Range (unit: Hz)
$D1(\cdot)$	12.5~25
$D2(\cdot)$	6.25~12.5
$D3(\cdot)$	3.125~6.25
$D4(\cdot)$	1.5625~3.125
$D5(\cdot)$	0.78125~1.5625

Legends:
1. The sampling frequency is 50 Hz.
2. Daubechies wavelet of order 6 (db6) is adopted in the signal decomposition.

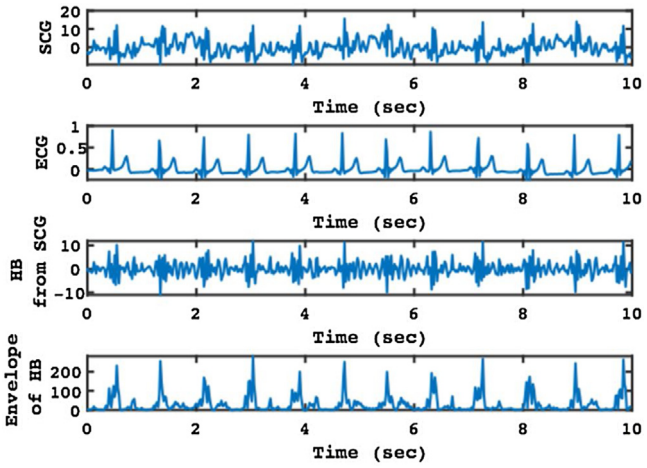

Fig. 4. The patterns related to heartbeat (HB) information acquired from SCG with the synchronously recorded ECG for the data numbered b017. Top: SCG; the second from top: ECG; the second from bottom: the HB pattern acquired from SCG; bottom: the envelope of HB.

The low-frequency and high-frequency components for wavelet decomposition are generally split by the dedicated lowpass filter and highpass filter that are termed as quadrature mirror filters (QMF). In this case, the frequency range covered by $AJ(\cdot)$ is 0 to $f_s/2^{J+1}$ Hz and that for $Dj(\cdot)$ is $f_s/2;^{j+1}$ to $f_s/2;^{j}$ Hz, with f_s represents the sampling frequency (in unit Hz) of the discrete-time sequence $s(\cdot)$ and $1 \le j \le J$ [43]. In this study, the sampling frequency of SCG signal is 50 Hz (will be described in Section 2.2) and J is 5. The corresponding frequency range for each decomposed component is summarized in Table 1. By inspecting on the pattern of SCG with respective to that of ECG (refer to the top and middle subfigures of Fig. 1), it can be observed that SCG is an oscillated signal that contains higher harmonics (more than 7) of the fundamental heartbeat component. This implies that the frequency range of heartbeat component acquired from SCG (denoted as HB from SCG) covers at least seven times of the fundamental heartbeat frequency which can be acquired by the beat-to-beat interval from ECG signal. As the fundamental heartbeat frequency is near around 1 Hz, HB from SCG may contain the components above 7 Hz and are therefore approximated by the sum of $D1(\cdot)$ and $D2(\cdot)$ in this research (refer to the covered frequency range for each decomposed component shown in Table 1). One example is illustrated in Fig. 4, which is for the case of data numbered b017 in CEBS database. In this figure, HB from SCG (the second subfigure from bottom) is the pattern for the sum of $D1(\cdot)$ and $D2(\cdot)$ from the wavelet decomposition of SCG signal. It can be observed that the timing of spikes in HB from SCG is synchronous to that of QRS complexes in ECG. As the spikes contain high-frequency oscillations, the envelope detection is required before further processing. The result of envelope detection for HB from SCG is shown simultaneously at the bottom subfigure of Fig. 4. The method for envelogram will be introduced in next subsection. In addition, as the normal respiratory frequency

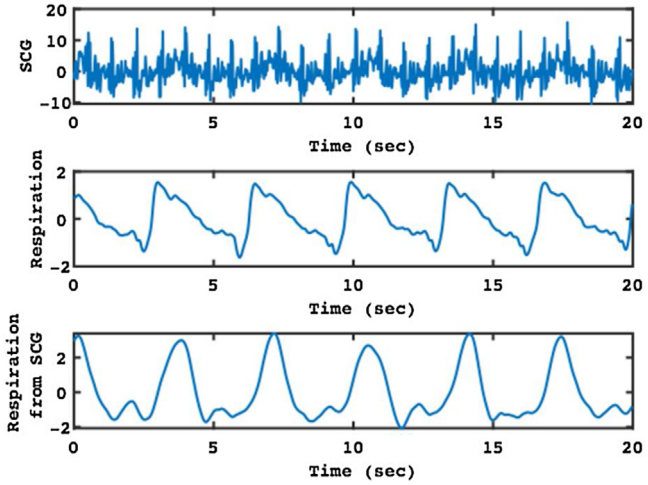

Fig. 5. The respiratory pattern acquired from SCG with the synchronously recorded respiratory signal for the data numbered b017. Top: SCG; middle: respiratory signal; bottom: the respiratory pattern acquired from SCG.

is located within 0.17~0.73 Hz [44], the component $A5(\cdot)$ is selected to acquire the respiratory information due to the coverage of respiratory frequency as refer to Table 1. Fig. 5 illustrates one example of the decomposed respiratory pattern from SCG (the bottom subfigure), also for the data numbered b017 in CEBS database. It can be observed that the pattern of respiration from SCG is in phase with that of practical respiratory signal measured with SCG synchronously.

2.1.2. Envelogram

As the heartbeat component acquired from SCG (denoted as HB from SCG) contains high-frequency oscillation, the envelope detection is required to derive a precise estimate on the heartbeat frequency (refer to Fig. 4). The envelogram proposed by Sarkady et al. [45] was adopted to obtain the envelope of HB from SCG in this study. Let $b(n)$ (with $1 \le n \le N$) represent the heartbeat component acquired from SCG, which is from $D1(\cdot) + D2(\cdot)$ by the 5-level db6 wavelet decomposition. The envelogram is derived by the following procedures.

Firstly, derive the discrete Fourier transform (DFT) of $b(n)$, which can be performed by fast Fourier transform (FFT). That is

$$B(k) = FFT\left\{b(n)\right\},\ 1 \le k \le N. \tag{3}$$

Next, re-arrange $B(k)$ by the following expression

$$B(k) = \begin{cases} B(k) \text{ for } k = 1 \\ 2 \cdot B(k) \text{ for } 2 \le k \le \dfrac{N}{2} + 1 \\ 0 \text{ for } \dfrac{N}{2} + 2 \le k \le N \end{cases} \tag{4}$$

Then, take the inverse DFT for the result derived in (4). Finally, the magnitude of the result gives the envelogram.

The bottom subfigure of Fig. 4 demonstrates the envelope of HB from SCG, and it can be observed that the pattern becomes smoother and the timing for peaks is also synchronous to that of QRS complexes in ECG.

2.1.3. Scalogram

The spectrum must be estimated for the envelope of HB (which is $D1(\cdot) + D2(\cdot)$ from SCG by wavelet decomposition) and for the respiratory component (which is $A5(\cdot)$ from SCG by wavelet decomposition) to derive the heartbeat frequency and the respiratory frequency such that HR and RR could be estimated respectively. Among various approaches for obtaining PSD, the scalogram by

complex Morlet wavelet is adopted in this study. This approach can be implemented by FFT and the PSD can also be conducted for the interested frequency range [17,46]. This is the reason why we selected this approach for the PSD estimation in this paper. The algorithm is briefly described as follows. For more detailed descriptions, the readers may refer to [17] or [46].

Let $x(n)$ (with $1 \le n \le N$) represent the signal to be analyzed with a sampling interval of T(sec). The reciprocal of T, which is the sampling frequency (in Hz), is presented by f_s. Its continuous-time counterpart is denoted by $x(t)$. The mother wavelet for complex Morlet wavelet is shown as follows

$$\phi\left(\frac{t-\tau}{s}\right) = (2\pi)^{-\frac{1}{2}} \cdot e^{j2\pi f \cdot \frac{t-\tau}{s}} \cdot e^{-\frac{(t-\tau)^2}{2s^2}}, \tag{5}$$

where the scale s represents the dilation factor and τ denotes the shifting factor. In continuous-time domain, the wavelet transform of signal $x(t)$ can be expressed as

$$W(s,t) = s^{-\frac{1}{2}} \cdot \left\{ x(t)^* \overline{\phi}\left(-\frac{t}{s}\right) \right\}, \tag{6}$$

in which the symbol $*$ denotes the convolution operator and the overbar notation means a complex conjugate. The corresponding discrete-time version for (6) is presented as follows

$$W(s,n) = s^{-\frac{1}{2}} \cdot \left\{ x(n) \circledast_N \overline{\phi}\left(-\frac{n \cdot T}{s}\right) \right\}, \tag{7}$$

where the symbol $\circledast_N$ stands for the N-point circular convolution. The computation can be conducted in an efficient way by FFT. The frequency-domain counterpart for (7) is presented by

$$FFT\left\{W(s,n)\right\} = s^{\frac{1}{2}} \cdot X(k) \cdot \frac{e^{-\frac{(s \cdot f_k - 1)^2}{2}}}{T}, \tag{8}$$

with

$$X(k) = FFT\left\{x(n)\right\},\ 1 \le k \le N, \tag{9}$$

and

$$f_k = \begin{cases} \dfrac{k-1}{N \cdot T} \text{ for } 1 \le k \le \dfrac{N}{2} + 1 \\ -\dfrac{k-1}{N \cdot T} \text{ for } \dfrac{N}{2} + 1 < k \le N \end{cases}. \tag{10}$$

Taking inverse FFT for (8), the wavelet transform for $x(n)$ at a specific value of s can then be derived. Such procedure is repeated for the assigned range of s as desired. This makes the wavelet transform a time-scale analysis in its essence. The relationship between the dilation factor s and the pseudo frequency f (in Hz) for complex Morlet wavelet is given as

$$f = \frac{f_s}{s}. \tag{11}$$

This implies that the wavelet transform by complex Morlet wavelet can be converted to be a time-frequency analysis by changing the scale s to the corresponding frequency according to (11). In this study, the approach of linear interpolation for the interested frequency range is adopted and the frequency resolution is selected to be 0.005 Hz. This selection makes an incremental resolution of 0.3 bpm (or rpm) for HR (or RR) estimation.

Having acquired $W(s,n)$ for every interested s, the scalogram, denoted as $S_c(f,n)$, can be derived by

$$S_c(f,n) = \left|W(s,n)\right|^2 \text{ with } s = \frac{f_s}{f}. \tag{12}$$

The scalogram is then time-averaged according to the following equation for each specified frequency f to obtain the time-averaged PSD

$$\overline{S_c}(f) = \frac{1}{N}\sum_{n=1}^{N} S_c(f,n). \tag{13}$$

The heartbeat frequency and respiratory frequency are obtained from the local maxima of time-averaged PSD for the range 0.05~0.73 and 0.75~1.7 Hz respectively. Multiplying these frequencies by 60, HR (in unit of beats per minute, bpm) and RR (in unit of respirations per minute, rpm) can then be derived. The processing procedure of the proposed algorithm is summarized in Fig. 6. From the previous description, the signal length, adopted decomposed component and frequency range utilized for the estimation of HR and RR are different. The envelogram is also included in HR estimation. Because the processing procedure for HR and RR estimation is somewhat different, the processing flows for HR and RR are illustrated separately in Fig. 6 (left: for HR estimation, right: for RR estimation) to avoid confusion and to keep the processing procedures clear enough.

As one purpose of this study is to propose the potential algorithm that is feasible to be implemented in the embedded system, the above algorithm is evaluated sequentially by a mode of segment-by-segment estimation. For the estimation of HR, a 10-second length of SCG (totally 500 points of data) is utilized for computation in the procedure each time. And then shift a certain time index with the same length of data for next estimation of HR. Such procedure is repeated till the end of signal. The procedure for the estimation of RR is conducted in a similar way. As the cycle of respiration is longer than heartbeat, it is a length of 20 s (totally 1000 points of data) adopted for RR estimation each time. The shifted time index is 50 (that is an interval of 1 s) for the sequential HR and RR estimation. In addition, another goal of this study is to evaluate the feasibility of the proposed algorithm by comparison with the results acquired from the gold standard approach. To reduce the bias induced by different approach, the values of HR (and RR) are also derived from the time-averaged PSD of ECG (and respiratory signal) by the same procedure mentioned above.

For Figs. 4 and 5, one issue to be noted is the timing difference among the signals. In terms of the heartbeat detection from SCG (refer to the upper two subfigures of Fig. 4), it can be observed that the timing of QRS complexes in ECG signal appears earlier than the spikes in SCG signal. This is reasonable as the QRS complex denotes the timing of ventricular contraction and ECG is a bioelectric signal that propagates at a faster speed than the propagation of mechanical wave such as SCG signal in the same transmission media (the thoracic tissues). In terms of the respiration detection from SCG (refer to Fig. 5), it is not easy to observe the timing difference as the respiratory component is buried inconspicuously in the SCG signal (refer to the top subfigure of Fig. 1). But it can be clearly observed that the respiratory signal (the middle subfigure of Fig. 5) has an apparent phase lead with respect to the respiratory pattern acquired from SCG (the bottom subfigure of Fig. 5). One possible reason may be resulted from the difference between the detection principle of the adopted sensors. The sensor adopted for respiratory signal in this research is a type of strain gauge, which is in its essence a flexible resistor that can reflect the respiratory pattern due to the variant resistance caused by the chest fluctuation during the respiration. However, the sensor for SCG signal is an accelerometer, which can estimate the value of acceleration that is caused by the thoracic motion in respiration from the detection of variant internal capacitance [20]. The R-C equivalent circuit formed by the internal capacitance of accelerometer and the input resistance of detection circuit in the sensor may cause a charging-discharging delay in the signal detection. There is no detailed information of exact measure-

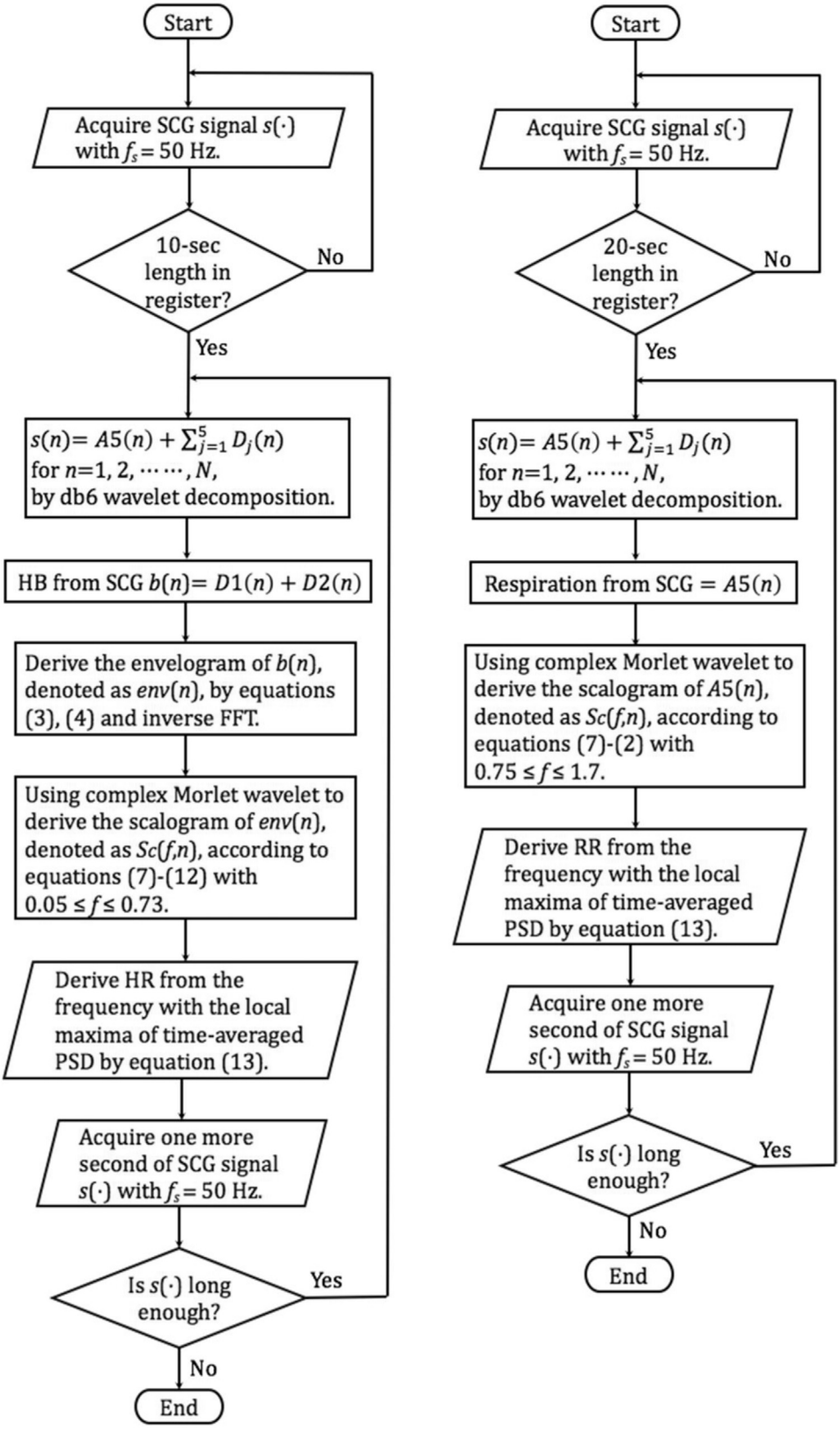

Fig. 6. Flowchart of the proposed algorithm. The left flowchart is for HR and the right flowchart is for RR.

ment site of SCG signal in the CEBS database. Although the position of SCG measurement in our self-conducted experiments is located at the aorta site, slight difference on the measurement site still exists for each subject. For this reason, this study does not dive into the detailed inspection on the phase difference between SCG versus ECG and respiratory signal. This paper only illustrates the phase shift caused by the proposed algorithm for SCG versus "Envelope of HB" and SCG versus "Respiration from SCG". The respective results

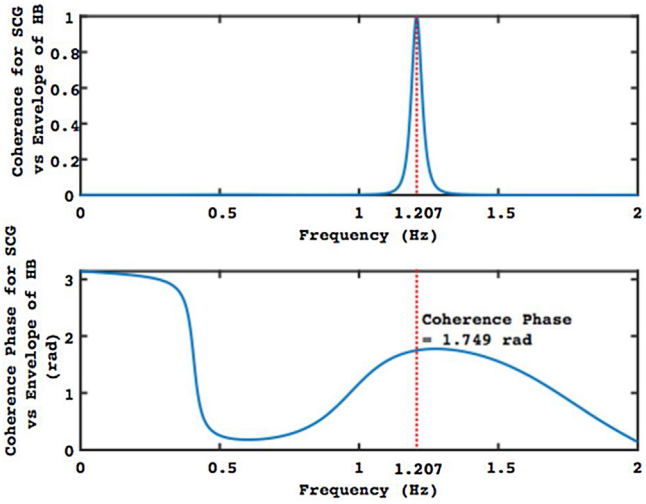

Fig. 7. Coherence (upper) and coherence phase (lower) for SCG versus the envelope of HB from SCG, for the signals shown in Fig. 4 (the pattern shown on top subfigure versus the pattern on bottom subfigure).

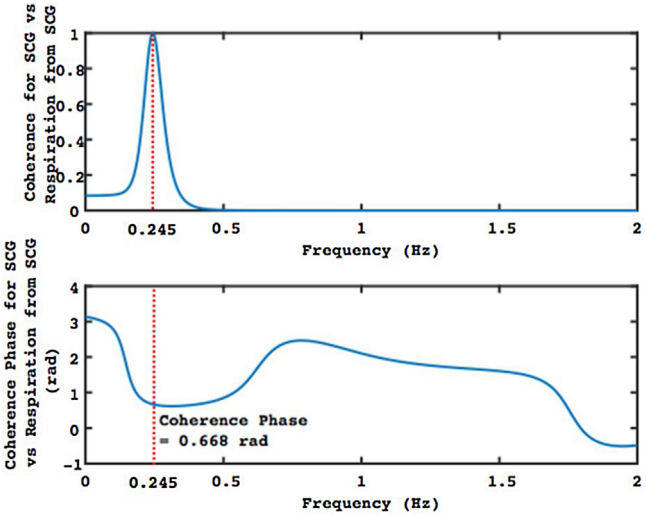

Fig. 8. Coherence (upper) and coherence phase (lower) for SCG versus the respiration from SCG, for the signals shown in Fig. 5 (the pattern shown on top subfigure versus the pattern on bottom subfigure.

are shown in Figs. 7 and 8. For these figures, the Vieira-Morf (VM) method is adopted for two-channel spectral estimation such that the phase difference between two signals could be estimated [47]. This is one approach for bivariate AR spectral estimation that can evaluate the coherence and coherence phase between two signals in higher frequency resolution under a shorter data length. Fig. 7 shows the coherence (upper) and coherence phase (lower) for the signals demonstrated in the top subfigure (SCG signal) and bottom subfigure (Envelope of HB) of Fig. 4, where the coherence phase is the phase of "Envelope of HB" with respect to that of SCG. From Fig. 7, it can be observed that SCG and "Envelope of HB" have the highest coherence at 1.207 Hz with a coherence phase of 1.749 rad here. This means that the SCG signal has a phase lead with respect to "Envelope of HB". This is reasonable because "Envelope of HB" is obtained by the procedure of wavelet decomposition and envelogram for SCG signal and this may lead to a phase lag for the resulted "Envelope of HB". Fig. 8 illustrates the coherence (upper) and coherence phase (lower) of the signals shown in the top subfigure (SCG signal) and bottom subfigure (Respiration from SCG) of Fig. 5, where the coherence phase is the phase of "Respiration from SCG" relative to that of SCG. From Fig. 8, it can be appreciated that SCG and "Respiration from SCG" have the greatest coherence at 0.245 Hz, and the coherence phase here is 0.668 rad. This implies that the SCG signal has a phase lead with respect to "Respiration from SCG". This is also reasonable because "Respiration from SCG" is obtained through the wavelet decomposition for SCG signal and this will cause a phase lag for the acquired "Respiration from SCG".

The most important computations for the proposed algorithm include the lowpass/highpass filtering by QMF [43] for db6 wavelet decomposition and FFT/inverse FFT for envelogram and scalogram. As both convolution (in the lowpass and highpass filtering) and inverse FFT can be performed by FFT [48], the resource needed for the embedded micro-controller unit (MCU) can be evaluated by the requirement for the computation of FFT. In the proposed algorithm, the data length in the estimation is 500 points for HR whereas it is 1000 points for RR. By appending zeros to the end of signals, the 512-point and 1024-point radix-2 FFT can be adopted respectively for HR and RR estimation. To minimize the requirement of computational resource in MCU, the estimation of HR and RR can be conducted alternately. For this reason, the resource for the computation of 1024-point FFT is a basic requirement for the selected MCU. Assume that one complex-valued data occupies the memory space of 4 bytes in the MCU. In this case, an amount of 4 K bytes is needed for the computation of one 1024-point FFT. Before derivation of the time-averaged PSD, the scalogram $S_c(f, n)$ must be acquired for every interested dilation factor s according to Eqs. (12) and (13). In this research, linear interpolation for the interested frequency range is adopted and the frequency resolution is 0.005 Hz. The corresponding frequency range for HR and RR detection is 0.75∼1.7 Hz and 0.05∼0.73, which includes 191 and 137 different frequencies respectively. Time-averaged PSD can be accomplished by the accumulated scalogram $S_c(f, n)$ at each distinct frequency, the practical requirement for memory space is 8 K bytes (one half for the computation of 1024-point FFT, another half for the storage of the accumulated scalogram). With extra memory space reserved for the storage of temporary variables and data during the computation, a memory space of 16 K bytes is required for the dedicated MCU. In addition, the MCU must also possess two analog-to-digital converters (A/D) and high-speed multiplier such that the proposed algorithm can be performed efficiently in the embedded system. The sampling frequency of the proposed algorithm is 50 Hz, which is easily realized for contemporary MCUs.

2.2. Materials and experiments

In this research, the CEBS database [21,22] from PhysioNet [23] is adopted to evaluate the feasibility of the proposed algorithms. This dataset was developed by the Electronic and Biomedical Instrumentation research group of Polytechnic University of Catalonia (UPC, Spain) with the ECG, breathing signal and SCG being measured simultaneously. The data were collected by the multifunction physiological data acquisition (DAQ) system MP36 (BIOPAC® Systems, Inc., USA). Twenty presumed healthy subjects (12 males and 8 females, aged between 19 and 30) were recruited in the experiments. Each subject was asked to keep quiet and awake in supine position on a bed and the data were recorded from the basal state (5 min, records b001 to b020), period of listening the classic music (50 min, records m001 to m020) until the post-resting state (5 min, records p001 to p020). Every record has two-channel ECG (lead I and lead II), one-channel respiration (by SS5LB sensor, BIOPAC® Systems, Inc., USA) and one-channel SCG (by LIS344ALH, STMicroelectronics) with the sampling frequency of 5000 Hz for each channel. SS5LB sensor is a strap-type strain gauge assembly that measures the change on thoracic or abdominal circumference due to respiration. The SCG sensor (LIS344ALH) is a high performance 3-axis accelerometer with user selectable full scale of $\pm 2\, g_0$

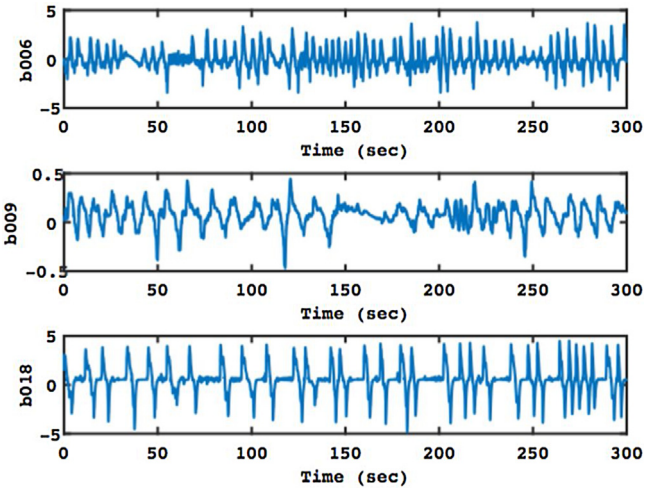

Fig. 9. Some patterns of irregular respiratory signal in the CEBS database.

or $\pm 6\ g_0$ and has the maximum bandwidth of 1800 Hz for all axes, where g_0 denotes the standard gravity (i.e. 9.8 m/sec^2). It has a sensitivity of (supply voltage)/5 (unit: V/g_0) for full-scale $\pm 2\ g_0$, and it is (supply voltage)/15 (unit: V/g_0) for full-scale $\pm 6\ g_0$. Another goal of this study is to develop the dedicated algorithm that can be adopted by the embedded system in the future. As the computational load for the original 5000-Hz sampling frequency is heavy for any micro-controller, the signals were downsampled to 50 Hz before further analysis. In this study, the SCG signals of 5-minute length in the CEBS database (records with character b or p prefix) were primarily used for the estimation of HR and RR, and the results were compared with those derived by the standard approaches. The records of 50-minute length (those withy character m prefix) were primarily used to verify the performance of the proposed algorithm in long-term tracing.

The quality of some respiratory signals in the CEBS database is not good enough for RR estimation. Some examples (but are not limited to these) are shown in Fig. 9. For these situations, it is not easy to estimate the value of RR, even by visual inspection. Because true RR values are not easily acquired in some records, the performance of RR estimation from SCG cannot be evaluated in these cases. To overcome this problem, the experiments similar to the CEBS database were also conducted in the university laboratory that is dedicated on the experiments of physiological measurement. Ten healthy subjects (3 males and 7 females, aged 23 ± 2 years) having no the record of cardiopulmonary diseases were recruited from the university. The conducted experiments were approved by the Regional Research Ethics Center of Taiwan (IRB approval number 201611044RINA) and written informed consent was obtained from all subjects. Similar to the experimental setup in CEBS database, the DAQ system MP30 (BIOPAC® Systems, Inc., USA) was utilized for the measurement of respiratory signal (by the respiration belt transducer SS5LB), lead II ECG (by the electrode lead set SS2L) and SCG (by MEMS triaxial analog accelerometer LIS344ALH, operated in full scale of $\pm 2\ g_0$, STMicroelectronics). Biopac Student Lab (BSL) analysis software was used for signal management and the sampling frequency for each channel was 50 Hz. Only the Z-channel signal of the accelerometer sensor was adopted for SCG in our experiments. This sensor was mounted on a flexible printed circuit board (FPCB) with a 50-cm wired bus and the bus lines were connected to the signal processing breadboard SS39 L (BIOPAC® Systems, Inc., USA). The specific cable SS60 L (BIOPAC® Systems, Inc., USA) for SS39 L was used to convey the sensed signal from the breadboard to the DAQ device MP30. The signals were acquired by the Biopac BSL software with the band-pass filtering of 0.05∼25 Hz. The sensor-mounted FPCB was placed at the position of subject chest having the most apparent heartbeat features with the QRS complexes of ECG as a timing reference. Before the experiments, each subject was asked to take full rest and to avoid the drinks with caffeine. The subject was kept in supine posture during signal measurement. Two kinds of experiment were performed on each subject, which are the paced breathing experiments and the spontaneous breathing experiment. In the paced breathing experiments, the subjects were requested to breathe according to the timing controlled by a metronome. The ratio of inspiratory duration to expiratory duration is 1:1. There are totally three paced breathing speeds in the experiments, which are 15 respiration per minute (rpm), 10 rpm and 5 rpm, respectively. In the spontaneous breathing experiment, the request for subjects were the breathing must be apparent and the posture must be kept as stable as possible. The experiments for each subject were conducted successively in the same morning with a separated interval of ten minutes at least and the duration for each experiment was five minutes.

2.3. Statistical analysis

In this study, two kinds of statistical analysis (ICC [38,39] and Bland-Altman agreement analysis [40]) were adopted to evaluate the feasibility of HR and RR acquired from SCG via the comparison with those obtained by conventional standard approaches.

ICC was originally proposed by R. Fisher to quantify the degree of relatedness for the case of paired measurements [38]. After the introduction of R. Fisher, a number of ICC statistics have been proposed and most of them are defined in terms of the random effects model. In this study, the MATLAB code developed by A. Salarian [49] was utilized for the estimation of ICC and 95 % confident intervals (C.I.). Salarian's MATLAB code is developed according to the literature by McGraw and Wong [39]. There are totally six types of ICC included in the code. Considering the conducted experiments in this study, the ICC of two-way mixed and single score (which is the type "A-1" in McGraw and Wong's convention) is selected for ICC computation. And, the lower and upper bounds of ICC were estimated under 0.05 level of significance. According to the guideline given by Koo and Li [50], a value of ICC below 0.50 represents poor agreement, 0.50 to 0.75 a moderate level, between 0.75 and 0.90 a good score, and it is excellent correlation for ICC above 0.90.

In clinical application, comparison of a new measurement technique with an established one is often needed to see whether they agree sufficiently for the new technique to replace the conventional one. The method proposed by Bland and Altman [40] is adopted to serve this purpose in this paper. Let the mean value for the differences between two measurement data be denoted as m_d and the standard deviation for the differences as s_d. A mean difference close to zero denotes a very high agreement between two measurements. The value of s_d can be used for a reference to see the variation between paired measurement data. The limits of agreement (with 95 % C.I.) are also derived to see the scattering characteristics in the measurement. The limits of agreement are given by $m_d - 2 \cdot s_d$ (lower) and $m_d + 2 \cdot s_d$ (upper). According to ANSI/AAMI EC13: 2000 (Sections 4.2.7 or 4.2.8.3), the minimal allowable HR meter range is 30–200 bpm, with an allowable error of no greater than ±10 percent of the input rate or ±5 bpm, whichever is greater [51]. As the latter one is a more rigorous requirement in general cases, ±5 bpm is selected to be the specification for HR estimation in this study. Taking the user's manual of contemporary patient monitor [52] as a reference, the error of RR within ±2 rpm compared with that from the standard device is selected to be the golden criterion of RR estimation. These specific values (±5 bpm for HR and ±2 rpm for RR) are used as an index to see whether the limits of agreement are within the defined ranges.

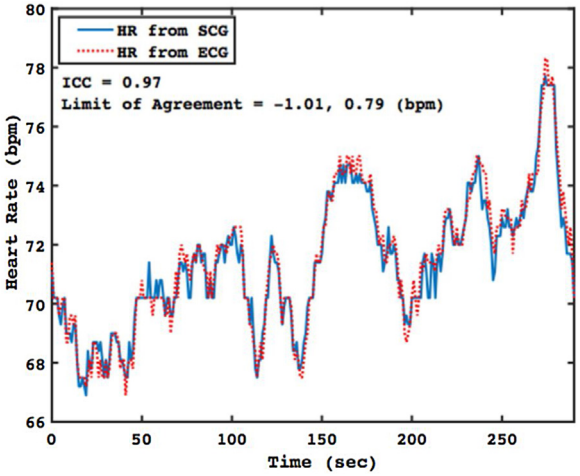

Fig. 10. The traces of HR estimation acquired from SCG (solid line) and ECG (dotted line) for the data numbered b017. The ICC and the lower and upper limit of agreement are also shown in the figure.

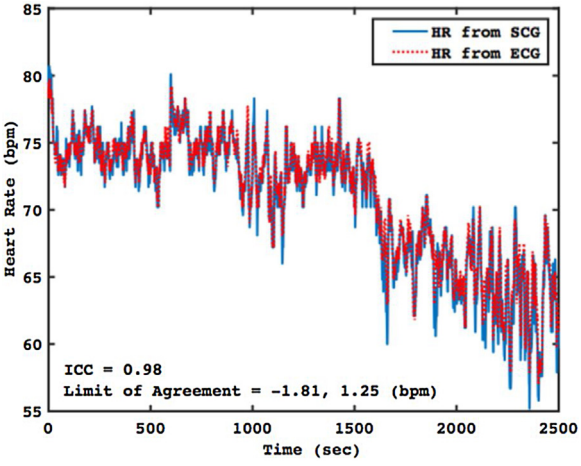

Fig. 11. The long-term traces of HR estimation acquired from SCG (solid line) and ECG (dotted line) for the data numbered m017. The ICC and the lower and upper limit of agreement are also shown in the figure.

3. Results and discussion

The computer analysis primarily consists of two parts. One is for the dataset of CEBS database, whereas another one is for the data collected from the experiments conducted in the university laboratory. For the analysis of CEBS database, the records of 5-minute length (those with character b or p prefix) are used for estimation of HR and RR, and the results were compared with those acquired by the standard approaches. Those of 50-minute length (the records with character m prefix) are mainly used to verify the performance of the proposed algorithm in long-term tracing. Because the statistical analysis may be influenced by the length of signal, only the results of 5-minute records are conducted for ICC computation and agreement analysis. These results are also summarized in tables to make the comparisons more convenient. To simplify the illustration, only one record is demonstrated by figures and the statistical results for 5-minute records are summarized by tables. Also, only one record is illustrated by figures in long-term (50-minute) sequential trace simulations.

Fig. 10 shows the sequential traces of HR acquired from SCG (solid line) and ECG (dotted line) for the record numbered b017. The HR estimation for sequential long-term trace for the same subject (017) is shown in Fig. 11. It can be observed that the results

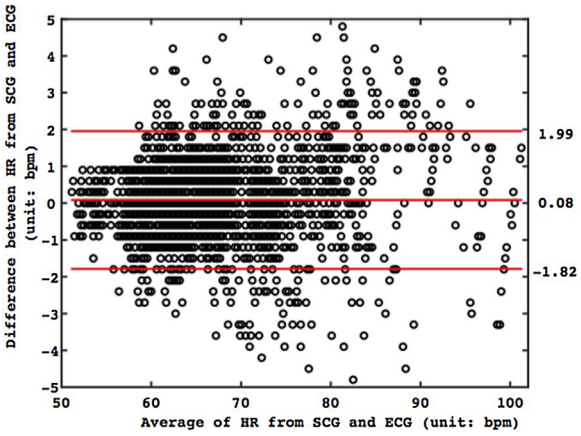

Fig. 12. Bland-Altman plot for HR estimation acquired from SCG and from ECG. Center solid line: mean difference between the two approaches. Upper and lower solid lines: *md* ±2·*sd* (95 % limits of agreement).

from SCG matches well with that from ECG in both figures. To quantify the matched degree, the value of ICC and the lower and upper limit of agreement are also illustrated in both figures. According to the guideline proposed by Koo and Li [49], the high values of ICC (0.97 and 0.98) in both records indicate an excellent correlation (greater than 0.90) for the HR estimation in different approaches. In addition, Fig. 12 shows the Bland-Altman plot for HR estimation from SCG and ECG. The results are derived from all of the records in CEBS database. Fig. 12 also shows the mean difference and the limits of agreement from all records in the dataset. The limits of agreement (−1.82 bpm, 1.99 bpm) satisfy the requirement given in ANSI/AAMI EC13: 2002 [51], which is within the specified range ±5 bpm. The statistical results for all 5-minute records are summarized in Table 2. From this table, the ICC values are at least 0.80 and the lowest 95 % C.I. is 0.75. According to Koo and Li's guideline [50], these statistical values indicate that the HR estimation have good to excellent correlation between the approaches by SCG and ECG. From this table, the worst limits of agreement for HR estimation are (−4.08 bpm, 2.43 bpm, for subject 018), and the values also satisfy the requirement of ANSI/AAMI EC13: 2002 [51].

From the results shown in Figures 10, 11, 12 and Table 2, it can be appreciated that the HR estimation from SCG by the proposed algorithm agrees well with that from ECG, the standard approach. This implies that the proposed algorithm is feasible to estimate HR from SCG. Or, HR can be estimated from SCG by the feasible algorithms.

The corresponding results for RR estimation are shown in Figs. 13–15 and Table 3. Fig. 13 demonstrates the RR estimation acquired from SCG (solid line) and respiratory signal (dashed line), also for the record numbered b017. The long-term sequential traces of RR estimation for the same subject (017) is demonstrated in Fig. 14. It can be found that the results from SCG matches well with that from respiratory signal for this subject. To quantify the matched degree, the value of ICC and the lower and upper limit of agreement are also illustrated in both figures. From the illustrated results for subject 017, the high values of ICC (0.97 and 0.99) denote the excellent correlation (greater than 0.90, refer to [50]) for the RR estimation in different approaches. In addition, Fig. 15 shows the Bland-Altman plot for RR estimation from SCG and respiratory signal. The results are also derived from all of the records in CEBS database. Fig. 15 also shows the mean difference and the limits of agreement from the whole dataset. The limits of agreement (−3.56 rpm, 3.98 rpm) do not satisfy the specification given in contemporary medical device [52], in which the error should not be beyond the specified range ±2 rpm as compared with the standard one. The results of statistical analysis for all 5-minute records are

Table 2
The summary of heart rate (HR) analysis for PhysioNet CEBS database.

Data	scgHR	ecgHR	ICC	95 % C. I. of ICC	Bias	Limit of Agreement
b001	63.98 ± 1.63	64.00 ± 1.72	0.93	0.92, 0.95	−0.02 ± 0.61	−1.23, 1.19
b002	60.32 ± 1.80	60.23 ± 1.72	0.94	0.93, 0.95	0.09 ± 0.59	−1.10, 1.28
b003	68.29 ± 2.61	67.49 ± 2.94	0.90	0.76, 0.95	0.80 ± 1.02	−1.25, 2.84
b004	63.37 ± 2.16	63.24 ± 1.92	0.94	0.92, 0.95	0.13 ± 0.73	−1.33, 1.60
b005	70.97 ± 1.91	70.88 ± 2.01	0.87	0.84, 0.90	0.10 ± 0.99	−1.88, 2.07
b006	60.36 ± 3.67	60.39 ± 3.73	0.98	0.97, 0.99	−0.03 ± 0.61	−1.25, 1.19
b007	53.19 ± 0.88	53.39 ± 0.89	0.81	0.75, 0.87	−0.21 ± 0.51	−1.23, 0.81
b008	94.10 ± 3.00	93.37 ± 3.21	0.85	0.78, 0.89	0.72 ± 1.89	−2.61, 4.05
b009	61.39 ± 3.26	61.18 ± 2.77	0.94	0.92, 0.95	0.21 ± 1.07	−1.92, 2.35
b010	60.21 ± 1.87	60.44 ± 1.66	0.80	0.75, 0.84	−0.23 ± 1.10	−2.42, 1.96
b011	65.31 ± 1.35	65.42 ± 1.34	0.85	0.81, 0.89	−0.10 ± 0.72	−1.55, 1.34
b012	78.84 ± 2.01	78.85 ± 2.29	0.84	0.81, 0.87	−0.02 ± 1.20	−2.43, 2.39
b013	70.39 ± 4.13	69.95 ± 3.83	0.94	0.92, 0.96	0.44 ± 1.27	−2.10, 2.98
b014	66.98 ± 1.68	67.25 ± 1.84	0.90	0.86, 0.93	−0.27 ± 0.74	−1.74, 1.20
b015	64.70 ± 2.53	64.72 ± 2.44	0.98	0.97, 0.99	−0.02 ± 0.45	−0.91, 0.87
b016	69.35 ± 2.49	68.90 ± 2.70	0.95	0.87, 0.98	0.45 ± 0.69	−0.92, 1.82
b017	71.35 ± 2.21	71.46 ± 2.32	0.97	0.96, 0.98	−0.11 ± 0.45	−1.01, 0.79
b018	79.88 ± 4.28	80.70 ± 4.43	0.91	0.85, 0.94	−0.82 ± 1.98	−4.08, 2.43
b019	61.66 ± 1.98	61.83 ± 1.68	0.92	0.90, 0.94	−0.17 ± 0.70	−1.56, 1.22
b020	65.31 ± 1.74	65.63 ± 1.64	0.94	0.84, 0.97	−0.32 ± 0.49	−1.30, 0.66
p001	63.51 ± 2.10	63.15 ± 1.92	0.92	0.85, 0.95	0.36 ± 0.73	−1.10, 1.83
p002	60.32 ± 1.80	60.23 ± 1.72	0.94	0.93, 0.95	0.09 ± 0.59	−1.10, 1.28
p003	68.29 ± 2.61	67.49 ± 2.94	0.90	0.76, 0.95	0.80 ± 1.02	−1.25, 2.85
p004	63.37 ± 2.16	63.24 ± 1.92	0.93	0.92, 0.95	0.13 ± 0.73	−1.33, 1.60
p005	70.97 ± 1.91	70.88 ± 2.02	0.87	0.84, 0.90	0.10 ± 0.99	−1.88, 2.08
p006	60.36 ± 3.67	60.39 ± 3.73	0.98	0.97, 0.99	−0.03 ± 0.61	−1.25, 1.19
p007	53.19 ± 0.88	53.39 ± 0.89	0.81	0.75, 0.87	−0.21 ± 0.51	−1.23, 0.81
p008	94.10 ± 3.00	93.37 ± 3.21	0.85	0.78, 0.89	0.72 ± 1.89	−2.61, 4.05
p009	61.39 ± 3.26	61.18 ± 2.77	0.94	0.92, 0.95	0.21 ± 1.07	−1.92, 2.35
p010	60.21 ± 1.87	60.44 ± 1.66	0.80	0.75, 0.84	−0.23 ± 1.10	−2.42, 1.96
p011	65.31 ± 1.35	65.42 ± 1.34	0.85	0.82, 0.89	−0.10 ± 0.72	−1.54, 1.34
p012	78.84 ± 2.01	78.85 ± 2.29	0.84	0.81, 0.87	−0.02 ± 1.21	−2.43, 2.39
p013	70.39 ± 4.13	69.95 ± 3.83	0.94	0.92, 0.96	0.44 ± 1.27	−2.01, 2.98
p014	66.98 ± 1.68	67.25 ± 1.84	0.90	0.86, 0.93	−0.27 ± 0.74	−1.74, 1.20
p015	64.70 ± 2.53	64.72 ± 2.44	0.98	0.97, 0.99	−0.02 ± 0.45	−0.91, 0.87
p016	69.35 ± 2.50	68.91 ± 2.70	0.95	0.87, 0.98	0.45 ± 0.69	−0.93, 1.82
p017	71.35 ± 2.21	71.46 ± 2.33	0.97	0.96, 0.98	−0.11 ± 0.45	−1.01, 0.79
p018	79.88 ± 4.08	80.70 ± 4.43	0.91	0.85, 0.94	−0.82 ± 1.98	−4.08, 2.43
p019	61.66 ± 1.98	61.83 ± 1.68	0.92	0.90, 0.94	−0.17 ± 0.70	−1.56, 1.22
p020	65.31 ± 1.74	65.63 ± 1.64	0.94	0.84, 0.97	−0.32 ± 0.49	−1.30, 0.66

Legends:
1. **scgHR** represents the heart rate (HR) derived from SCG, and **ecgHR** represents the HR acquired from ECG. Both are presented as mean ± standard deviation (SD). The unit is beat per minute (bpm).
2. **ICC** means the intraclass correlation coefficient. **C. I.** is the abbreviation of confident interval.
3. **Bias** denotes the difference between each **scgHR** and **ecgHR** pair presented as mean ± SD with the unit of bpm.
4. **Limit of Agreement** denotes the lower and the upper limit of agreement for the Bland-Altman agreement analysis between **scgHR** and **ecgHR** with the unit of bpm.

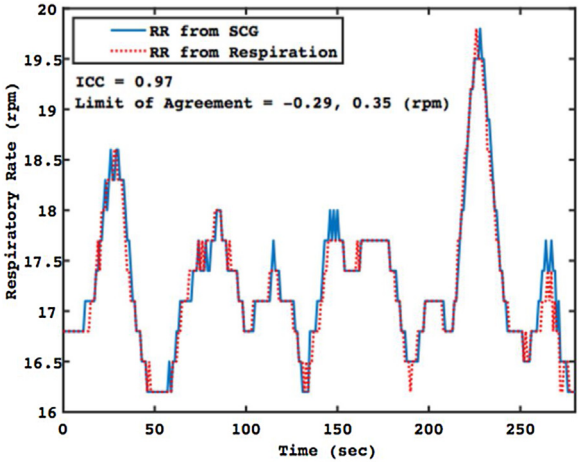

Fig. 13. The traces of RR estimation acquired from SCG (solid line) and respiratory signal (dotted line) for the data numbered b017. The ICC and the lower and upper limit of agreement are also shown in the figure.

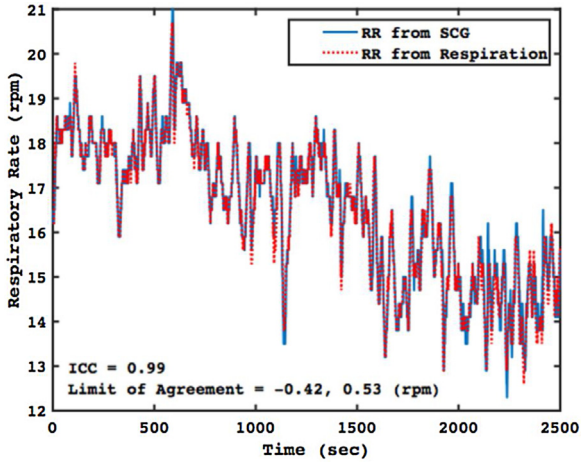

Fig. 14. The long-term traces of RR estimation acquired from SCG (solid line) and respiratory signal (dotted line) for the data numbered m017. The ICC and the lower and upper limit of agreement are also shown in the figure.

Table 3
The summary of respiratory rate (RR) analysis for PhysioNet CEBS database.

Data	scgRR	respRR	ICC	95 % C. I. of ICC	Bias	Limit of Agreement
b001	21.27 ± 0.72	21.14 ± 0.68	0.91	0.83, 0.95	0.14 ± 0.27	−0.40, 0.67
b002	16.23 ± 1.82	16.44 ± 1.73	0.95	0.92, 0.96	−0.21 ± 0.54	−1.30, 0.88
b003	15.89 ± 0.79	15.96 ± 0.82	0.95	0.93, 0.96	−0.07 ± 0.25	−0.57, 0.42
b004 †	14.26 ± 2.05	14.24 ± 1.04	0.38	0.28, 0.48	0.03 ± 1.81	−3.59, 3.64
b005	15.56 ± 1.01	15.68 ± 0.83	0.85	0.81, 0.89	−0.13 ± 0.49	−1.11, 0.86
b006 †	11.36 ± 5.05	13.12 ± 2.26	0.42	0.24, 0.56	−1.77 ± 3.72	−9.21, 5.68
b007 †	12.33 ± 2.79	11.22 ± 1.84	0.48	0.29, 0.62	1.11 ± 2.28	−3.45, 5.68
b008	22.51 ± 1.57	22.35 ± 1.62	0.96	0.94, 0.97	0.15 ± 0.44	−0.72, 1.03
b009 †	8.03 ± 3.55	6.56 ± 2.08	0.32	0.17, 0.45	1.48 ± 3.29	−5.10, 8.05
b010 †	16.06 ± 5.76	14.08 ± 1.95	0.39	0.22, 0.53	1.98 ± 4.60	−6.21, 10.17
b011	14.10 ± 1.11	13.86 ± 1.14	0.84	0.76, 0.89	0.24 ± 0.60	−0.96, 1.43
b012	22.42 ± 1.45	22.59 ± 1.22	0.89	0.85, 0.91	−0.16 ± 0.62	−1.41, 1.08
b013	20.33 ± 1.21	20.23 ± 1.10	0.91	0.88, 0.93	0.09 ± 0.49	−0.89, 1.08
b014	15.49 ± 1.78	15.31 ± 1.59	0.86	0.82, 0.89	0.18 ± 0.89	−1.61, 1.97
b015 †	18.53 ± 1.74	17.71 ± 1.09	0.46	0.20, 0.63	0.82 ± 1.42	−3.01, 4.65
b016 †	15.92 ± 4.49	14.10 ± 3.82	0.57	0.38, 0.70	1.81 ± 3.61	−5.40, 9.03
b017	17.26 ± 0.70	17.23 ± 0.69	0.97	0.96, 0.98	0.03 ± 0.16	−0.29, 0.35
b018 †	9.53 ± 3.96	8.74 ± 2.69	0.50	0.39, 0.59	0.79 ± 3.35	−5.92, 7.50
b019	21.14 ± 1.14	21.07 ± 1.09	0.98	0.97, 0.99	0.08 ± 0.22	−0.36, 0.52
b020	11.71 ± 1.45	11.86 ± 1.52	0.91	0.88, 0.93	−0.15 ± 0.61	−1.38, 1.08
p001	18.81 ± 0.79	18.69 ± 0.77	0.95	0.90, 0.97	0.12 ± 0.23	−0.35, 0.58
p002	16.23 ± 1.82	16.44 ± 1.73	0.95	0.92, 0.96	−0.21 ± 0.54	−1.30, 0.88
p003	15.89 ± 0.79	15.96 ± 0.82	0.95	0.93, 0.96	−0.07 ± 0.25	−0.57, 0.42
p004 †	14.26 ± 2.05	14.24 ± 1.04	0.38	0.28, 0.48	0.03 ± 1.81	−3.59, 3.64
p005	15.56 ± 1.01	15.68 ± 0.83	0.85	0.81, 0.89	−0.13 ± 0.49	−1.11, 0.86
p006 †	11.36 ± 5.05	13.12 ± 2.26	0.42	0.24, 0.56	−1.77 ± 3.72	−9.21, 5.68
p007 †	12.33 ± 2.79	11.22 ± 1.84	0.48	0.29, 0.62	1.11 ± 2.28	−3.45, 5.68
p008	22.51 ± 1.57	22.35 ± 1.62	0.96	0.94, 0.97	0.15 ± 0.44	−0.72, 1.03
p009 †	8.03 ± 3.55	6.56 ± 2.09	0.32	0.17, 0.45	1.48 ± 3.29	−5.10, 8.05
p010 †	16.06 ± 5.76	14.08 ± 1.95	0.39	0.22, 0.53	1.98 ± 4.60	−6.21, 10.17
p011	14.10 ± 1.11	13.86 ± 1.14	0.84	0.76, 0.89	0.24 ± 0.60	−0.96, 1.43
p012	22.42 ± 1.45	22.59 ± 1.22	0.89	0.85, 0.91	−0.16 ± 0.62	−1.41, 1.08
p013	20.32 ± 1.21	20.23 ± 1.10	0.91	0.88, 0.93	0.09 ± 0.49	−0.88, 1.07
p014	15.49 ± 1.78	15.31 ± 1.59	0.86	0.82, 0.89	0.18 ± 0.89	−1.60, 1.97
p015 †	18.53 ± 1.74	17.71 ± 1.09	0.46	0.20, 0.63	0.82 ± 1.42	−3.01, 4.65
p016 †	15.92 ± 4.49	14.10 ± 3.82	0.57	0.38, 0.70	1.81 ± 3.61	−5.40, 9.03
p017	17.26 ± 0.70	17.23 ± 0.69	0.97	0.96, 0.98	0.03 ± 0.16	−0.29, 0.35
p018 †	9.54 ± 3.96	8.74 ± 2.69	0.50	0.39, 0.59	0.79 ± 3.36	−5.92, 7.50
p019	21.14 ± 1.14	21.07 ± 1.09	0.98	0.97, 0.99	0.08 ± 0.22	−0.36, 0.52
p020	11.71 ± 1.45	11.86 ± 1.52	0.91	0.88, 0.93	−0.15 ± 0.61	−1.38, 1.08

Legends:
1. **scgRR** represents the respiratory rate (RR) derived from SCG, and **respRR** represents the RR acquired from respiratory signal. Both are presented as mean ± standard deviation (SD). The unit is respiration per minute (rpm).
2. **ICC** means the intraclass correlation coefficient. **C. I.** is the abbreviation of confident interval.
3. **Bias** denotes the difference between each **scgRR** and **respRR** pair presented as mean ± SD with the unit of rpm.
4. **Limit of Agreement** denotes the lower and the upper limit of agreement for the Bland-Altman agreement analysis between **scgRR** and **respRR** with the unit of rpm.
5. The symbol † indicates the allowable limit of agreement for RR estimation is beyond ±2 rpm.

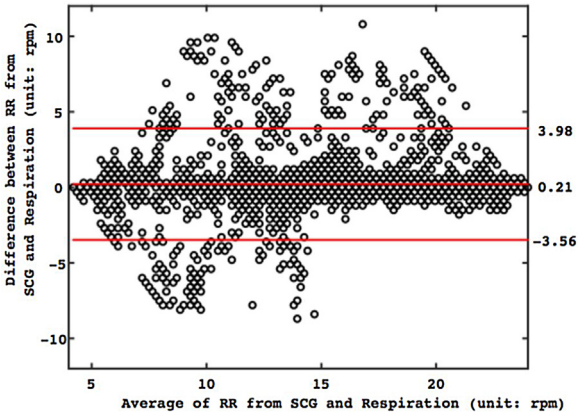

Fig. 15. Bland-Altman plot for the RR estimation acquired from SCG and from respiratory signal. Center solid line: mean difference between the two approaches. Upper and lower solid lines: *md* ±2·*sd* (95 % limits of agreement).

summarized in Table 3. From this table, the ICC values are located in the range 0.32∼0.98 and the lowest 95 % C.I. is 0.17. By Koo and Li's guideline [50], these statistical values indicate that the RR estimation is of poor to excellent correlation between the approaches by SCG and respiratory signal.

From the results shown in Figs. 13–15 and Table 3, it can be observed that the RR estimation from SCG (by the proposed algorithm) and that from respiratory signal (the standard approach) agree well only for some signals in the CEBS database. Not all of the analysis results possess high-degree correlation. The reason may be resulted from the irregular respiratory pattern in some subjects (refer to Fig. 9). The value of RR is not easily estimated even by visual inspection from the respiratory signal in these cases, which may lead to an erroneous estimation on RR value. In order to validate whether it is feasible to estimate RR from SCG, the experiments of spontaneous and paced breathing rate have been conducted in the university laboratory (refer to Section 2.2 for more detailed description). The purpose is to collect the respiratory signals of high quality under a standard operating procedure (SOP). The results of RR estimation for the experiments are summarized in Table 4. From this table, the ICC values are located in the range 0.84∼0.98 and the lowest 95 % C.I. is 0.81, and this implies the correlation of

Table 4
The summary of respiratory rate (RR) analysis for ten recruited subjects.

Status	Subject	scgRR	respRR	ICC	95 % C. I. of ICC	Bias	Limit of Agreement
Paced 15 rpm	F01	14.63 ± 0.20	14.66 ± 0.16	0.87	0.84, 0.92	0.00 ± 0.09	−0.18, 0.18
	F02	14.72 ± 0.38	14.68 ± 0.36	0.89	0.84, 0.93	0.04 ± 0.17	−0.30, 0.38
	F03	14.64 ± 0.23	14.68 ± 0.21	0.86	0.83, 0.90	−0.03 ± 0.11	−0.25, 0.19
	F04	14.67 ± 0.24	14.68 ± 0.23	0.88	0.83, 0.92	−0.00 ± 0.11	−0.23, 0.22
	F05	14.70 ± 0.40	14.70 ± 0.40	0.97	0.96, 0.98	0.00 ± 0.10	−0.20, 0.20
	F06	14.56 ± 0.35	14.58 ± 0.40	0.94	0.92, 0.96	−0.02 ± 0.12	−0.26, 0.23
	F07	14.52 ± 0.19	14.51 ± 0.19	0.84	0.81, 0.92	0.00 ± 0.11	−0.22, 0.23
	M01	14.52 ± 0.32	14.58 ± 0.29	0.86	0.82, 0.92	−0.07 ± 0.15	−0.37, 0.24
	M02	14.38 ± 0.78	14.52 ± 0.89	0.90	0.82, 0.94	−0.14 ± 0.36	−0.86, 0.58
	M03	14.76 ± 0.64	14.83 ± 0.60	0.93	0.89, 0.95	−0.07 ± 0.23	−0.53, 0.39
Paced 10 rpm	F01	9.79 ± 0.46	9.79 ± 0.40	0.95	0.93, 0.96	0.00 ± 0.14	−0.28, 0.28
	F02	10.00 ± 0.43	10.01 ± 0.46	0.90	0.86, 0.92	−0.02 ± 0.20	−0.42, 0.39
	F03	9.94 ± 0.73	9.98 ± 0.69	0.97	0.95, 0.98	−0.04 ± 0.18	−0.40, 0.31
	F04	9.48 ± 0.68	9.54 ± 0.58	0.88	0.82, 0.93	−0.07 ± 0.30	−0.66, 0.53
	F05	9.82 ± 0.26	9.83 ± 0.22	0.88	0.84, 0.91	−0.01 ± 0.12	−0.25, 0.22
	F06	9.63 ± 0.54	9.73 ± 0.52	0.86	0.82, 0.90	−0.10 ± 0.30	−0.70, 0.51
	F07	9.94 ± 0.32	9.95 ± 0.35	0.92	0.84, 0.96	−0.02 ± 0.14	−0.29, 0.25
	M01	9.76 ± 0.36	9.71 ± 0.36	0.94	0.83, 0.98	0.05 ± 0.11	−0.17, 0.28
	M02	9.76 ± 0.50	9.78 ± 0.45	0.91	0.85, 0.95	−0.01 ± 0.20	−0.41, 0.39
	M03	9.67 ± 0.45	9.68 ± 0.48	0.87	0.82, 0.92	−0.02 ± 0.24	−0.50, 0.46
Paced 5 rpm	F01	5.04 ± 0.35	5.05 ± 0.32	0.88	0.83, 0.91	−0.02 ± 0.17	−0.35, 0.32
	F02	5.13 ± 0.38	5.12 ± 0.33	0.86	0.82, 0.91	0.01 ± 0.19	−0.36, 0.39
	F03	5.01 ± 0.17	5.01 ± 0.16	0.92	0.88, 0.94	−0.00 ± 0.07	−0.14, 0.13
	F04	5.04 ± 0.21	5.04 ± 0.18	0.90	0.85, 0.94	0.00 ± 0.09	−0.17, 0.17
	F05	5.06 ± 0.15	5.05 ± 0.15	0.87	0.83, 0.91	0.01 ± 0.08	−0.15, 0.16
	F06	4.98 ± 0.59	5.00 ± 0.58	0.93	0.90, 0.95	−0.02 ± 0.23	−0.47, 0.44
	F07	5.04 ± 0.62	5.12 ± 0.57	0.91	0.85, 0.95	−0.08 ± 0.24	−0.56, 0.41
	M01	5.31 ± 0.47	5.31 ± 0.45	0.93	0.86, 0.97	0.00 ± 0.17	−0.35, 0.35
	M02	5.10 ± 0.38	5.08 ± 0.35	0.87	0.84, 0.91	0.02 ± 0.19	−0.36, 0.40
	M03	5.13 ± 0.08	5.11 ± 0.07	0.86	0.82, 0.93	0.02 ± 0.04	−0.06, 0.09
Spontaneous	F01	9.18 ± 1.17	9.09 ± 1.16	0.89	0.85, 0.91	0.08 ± 0.55	−1.02, 1.18
	F02	14.07 ± 1.47	14.19 ± 1.37	0.91	0.89, 0.93	−0.12 ± 0.58	−1.28, 1.03
	F03	5.99 ± 0.47	6.00 ± 0.46	0.89	0.86, 0.91	−0.01 ± 0.22	−0.44, 0.43
	F04	8.95 ± 1.13	9.02 ± 1.16	0.92	0.90, 0.94	−0.07 ± 0.45	−0.98, 0.83
	F05	12.54 ± 0.76	12.56 ± 0.77	0.98	0.97, 0.99	−0.02 ± 0.12	−0.27, 0.22
	F06	16.49 ± 2.00	16.53 ± 1.98	0.97	0.96, 0.99	−0.04 ± 0.19	−0.43, 0.34
	F07	17.10 ± 0.99	17.12 ± 1.07	0.92	0.89, 0.94	−0.02 ± 0.42	−0.85, 0.82
	M01	12.87 ± 0.91	12.95 ± 0.95	0.91	0.89, 0.93	−0.08 ± 0.38	−0.84, 0.69
	M02	7.82 ± 0.99	7.78 ± 0.96	0.91	0.89, 0.93	0.04 ± 0.40	−0.76, 0.85
	M03	12.57 ± 1.81	12.73 ± 1.65	0.88	0.84, 0.92	−0.16 ± 0.83	−1.82, 1.50

Legends:
1. **scgRR** represents the respiratory rate (RR) derived from SCG, and **respRR** represents the RR acquired from respiratory signal. Both are presented as mean ± standard deviation (SD). The unit is respiration per minute (rpm).
2. **ICC** means the intraclass correlation coefficient. **C. I.** is the abbreviation of confident interval.
3. **Bias** denotes the difference between each **scgRR** and **respRR** pair presented as mean ± SD with the unit of rpm.
4. **Limit of Agreement** denotes the lower and the upper limit of agreement for the Bland-Altman agreement analysis between **scgRR** and **respRR** with the unit of rpm.

good to excellent level (by Koo and Li's guideline [50]) between the approaches of RR estimation by SCG and by respiratory signal. In addition, the worst limits of agreement for RR estimation are (−1.82 rpm, 1.50 rpm), and the values also satisfy the specification given in contemporary medical device [52]. The results indicate that the proposed algorithm is not only feasible to estimate HR from SCG but also feasible to estimate RR from SCG. And, we can also say that RR can be estimated from SCG by the feasible algorithms.

As the RR estimation is not ideal for all of the records in CEBS database, the extra experiments have been conducted in the university laboratory under well-controlled procedure. The results of statistical analysis reflect the correlation of good to excellent level between two approaches and the limits of agreement also meet the specification of contemporary medical device. This implies the measurement of SCG may need further care on signal quality and operating procedure such that the reliable estimation could be obtained, especially for the case of RR estimation. In addition, the visual inspection on signal quality is utilized in our operating procedure. The position of sensor placement is somewhat different for each person in the experiments. This may be resulted from the specific difference on the body shape and the quantity of body fat for each subject. Another constraint of this study is that the proposed algorithm does not consider the motion artifact. The primary reason is that the signals in CEBS database are collected under resting state (in supine posture). The removal of motion artifact needs additional processing procedure such that the estimation of HR and RR could be acquired. Recovering the clean signal from the motion artifact is another important topic in biomedical signal processing. For such kind of research, however, it is not easy to validate the correctness of the recovered pattern for the experiments with subject motion. Especially, there is no standard database with ECG, respiratory signal and SCG being corrupted by motion artifact yet the important fiducial points on the signals have been annotated by experts, which makes the verification of the estimated result a difficult task. For these reasons, the performance of algorithm can only be evaluated in a reliable way for the datasets collected under resting state at present time. This is why the proposed algorithm is dedicated only to the usage for the SCG signal measured under resting state. The practical application in clinical setting is suggested to be utilized primarily for the cases of patient in quiescent status such as those in vegetative state, in ICU, during the surgery or in sleep monitoring, and so on.

For the system implementation, some matters have to be noted in practical use. The first one is that the sensitivity of adopted accelerometer must be at least (supply voltage)/5 (unit: V/g_0, because this is the sensitivity of the accelerometer adopted in this

research). In addition, as the net weight of the sensor system may affect the measurement sensitivity, the sensor system must be kept as light-weighted as possible. To attain the goal, the number of utilized components in the sensor system must be as few as possible and using FPCB (flexible printed circuit board) may be beneficial to lower down the total weight. Finally, to increase the signal quality of SCG measurement, the sensor system can be pasted fixedly by medical adhesive tape at the position with the most apparent heart sound and respiratory sound. In our experience, one feasible position is on the second intercostal space at the right sternal margin (the aorta site). This is one position where both heartbeat and respiration are relatively obvious on the chest. Please also note that only healthy subjects were included in our research, the measurement site for patients may not be the same as that for healthy subjects, especially for the patients of heart disease and chronic obstructive pulmonary disease (COPD). In clinical setting, using the stethoscope can be helpful to find the proper position.

4. Conclusion

This paper presents an algorithm to estimate HR and RR simultaneously from SCG. The proposed algorithm can be coded in an efficient way and is feasible to be implemented in an embedded system. In addition to using the CEBS database, this study has also implemented the SCG sensor system and conducted physiological experiments to obtain high-quality signals under resting state. The acquired signals have been used to evaluate the feasibility of RR estimation from SCG. The estimations acquired from SCG have compared with those derived by the respective gold standard approach and have been tested by rigorous statistical tests.

For HR estimation, the minimal ICC value is 0.80 and the 95 % C.I. is at least 0.75. These statistical values indicate good to excellent correlation between the approaches by SCG and ECG. Also, even the worst limits of agreement for HR estimation (which is −4.08 bpm, 2.43 bpm) satisfy the requirement of the maximal allowable error, ±5 bpm, for the HR meter. As the quality of some respiratory signals in the CEBS database is not good for RR estimation, the extra experiments have been conducted in the university laboratory that is dedicated on the experiments of physiological measurement under well-controlled procedure. For the RR estimation of these experiments, the ICC values are located in the range 0.84∼0.98 and the lowest 95 % C.I. is 0.81. This indicates good to excellent correlation between the approaches of RR estimation by SCG and respiratory signal. In addition, the worst limits of agreement for RR estimation are (−1.82 rpm, 1.50 rpm), and the values also meet the specification given in contemporary medical device (which is ±2 rpm).

The above results indicate that HR and RR can be estimated from SCG. To date, there is no standard database with ECG, respiratory signal and SCG being measured during motion and simultaneously the important fiducial points on the signals being annotated by experts. This makes the verification of estimation for the cases with motion artifact a difficult task. At present time, the proposed algorithm is only focused on the usage under resting state. In clinical settings, the proposed technology may be potential for the patients under quiescent status such as those in vegetative state, in ICU, during the surgery or in sleep monitoring, and so on. Such approach can be incorporated in a unique embedded device to make the estimation of HR and RR in a simpler way than ever.

Acknowledgement

The authors wish to express the appreciation to the Ministry of Science and Technology of Taiwan (contract number: MOST 106-2221-E-035-024-MY2 and 108-2221-E-035-032) for the financial support on this research.

Declaration of Competing Interest

The authors hereby declare that there is no conflict of interest.

References

[1] W.B. Kannel, C. Kannel, R.S. Paffenbarger, L.A. Cupples, Heart rate and cardiovascular mortality: the Framingham study, Amer. Heart J. 113 (6) (1987) 1489–1494.
[2] E. Thaulow, J.E. Erikssen, How important is heart rate? J. Hypertens. Suppl. 9 (7) (1991) 27–30.
[3] K. Fox, J.S. Borer, A.J. Camm, N. Danchin, R. Ferrari, J.L. Sendon, P.G. Steg, J.C. Tardif, L. Tavazzi, M. Tendera, Resting heart rate in cardiovascular disease, J. Amer. Coll. Cardiol. 50 (9) (2007) 823–830.
[4] A. Diaz, M.G. Bourassa, M.C. Guertin, J.C. Tardif, Long-term prognostic value of resting heart rate in patients with suspected or proven coronary artery disease, Eur. Heart J. 26 (10) (2005) 967–974.
[5] J.F. Fieselmann, M.S. Hendryx, C.M. Helms, D.S. Wakefield, Respiratory rate predicts cardiopulmonary arrest for internal medicine inpatients", J. Gen. Intern. Med. 8 (1993) 354–360.
[6] M.A. Cretikos, R. Bellomo, K. Hillman, J. Chen, S. Finfer, A. Flabouris, Respiratory rate: the neglected vital sign, Med. J. Australia 188 (11) (2008) 657–659.
[7] K. Mochizuki, R. Shintani, K. Mori, T. Sato, O. Sakaguchi, K. Takeshige, K. Nitta, H. Imamura, Importance of respiratory rate for the prediction of clinical deterioration after emergency department discharge: a single-center, case-control study, Acute Med. Surg. 4 (2) (2017) 172–178.
[8] C. Kelly, Respiratory rate 1: why measurement and recording are crucial, Nurs. Times 114 (4) (2018) 23–24.
[9] R. Ortega, C. Connor, S. Kim, R. Djang, K. Patel, Monitoring ventilation with capnography, New England J. Med. Surg. Collat. Branches Sci. 367 (19) (2012) e27.
[10] R.D. Allison, E.L. Holmes, J. Nyboer, Volumetric dynamic of respiration as measured by electrical impedance plethysmography, J. Appl. Physiol. 19 (1964) 166–173.
[11] G.B. Moody, R.G. Mark, A. Zoccola, S. Mantero, Derivation of respiratory signals from multi-lead ECGs, Comput. Cardiol. 12 (1985) 113–116.
[12] A.M. Cyna, V. Kulkarni, M.E. Tunstall, J.M.S. Hutchinson, J.R. Mallard, Aura: a new respiratory monitoring and apnea alarm for spontaneously breathing patients, Br. J. Anaesth. 67 (1991) 341–345.
[13] G.B. Drummond, A. Bates, J. Mann, D.K. Arvind, Validation of a new non-invasive automatic monitor of respiratory rate for postoperative subjects, Br. J. Anaesth. 107 (3) (2011) 462–469.
[14] K. Pandia, O.T. Inan, G.T.A. Kovacs, L. Giovangrandi, Extracting respiratory information from seismocardiogram signals acquired on the chest using a miniature accelerometer, Physiol. Meas. 33 (10) (2012) 1643–1660.
[15] O. Mimoz, T. Benard, A. Gaucher, D. Frasca, B. Debaene, Accuracy of respiratory rate monitoring using a non-invasive acoustic method after general anaesthesia, Br. J. Anaesth. 108 (5) (2012) 872–875.
[16] X. Zhang, Q. Ding, Respiratory rate estimation from the photoplethysmogram via joint sparse signal reconstruction and spectral fusion, Biomed. Signal Process. Control 35 (2017) 1–7.
[17] Y.D. Lin, Y.H. Chien, Y.S. Chen, Wavelet-based embedded algorithm for respiratory rate estimation from PPG signal, Biomed. Signal Process. Control 36 (2017) 138–145.
[18] E. Zimlichman, M. Szyper-Kravitz, A. Untertan, A. Goldman, S. Levkovich, Y. Shoenfeld, How is my patient doing? Evaluating hospitalized patients using continuous vital signs monitoring, Isr. Med. Assoc. J. 11 (2009) 382–384.
[19] H. Brown, J. Terrence, P. Vasquez, D.W. Bates, E. Zimlichman, Continuous monitoring in an inpatient medical-surgical unit: a controlled clinical trial, Amer. J. Med. 127 (2014) 226–232.
[20] N. Yazdi, F. Ayazi, K. Najafi, Micromachined inertial sensors, Proc. IEEE 86 (8) (1998) 1640–1659.
[21] M.A. García-González, A. Argelagós-Palau, M. Fernández-Chimeno, J. Ramos-Castro, A comparison of heartbeat detectors for seismocardiogram, Comput. Cardiol. 40 (2013) 461–464.
[22] M.A. García-González, A. Argelagós-Palau, M. Fernández-Chimeno, J. Ramos-Castro, Differences in QRS locations due to ECG lead: relationship with breathing XIII Mediterranean Conference on Medical and Biological Engineering and Computing 2013, IFMBE Proc., 41, 2013, pp. 962–964.
[23] A.L. Goldberger, L.A. Amaral, L. Glass, J.M. Hausdorff, P.C. Ivanov, R.G. Mark, J.E. Mietus, G.B. Moody, C.K. Peng, H.E. Stanley, PhysioBank, PhysioToolkit, and PhysioNet: components of a new research resource for complex physiologic signals, Circulation 101 (23) (2000) e215–e220.
[24] J.P. Burg, Maximum Entropy Spectral Analysis, May 1975. Stanford University Ph.D. dissertation. Available online: http://sepwww.stanford.edu/data/media/public/oldreports/sep06/.
[25] M. Jafari Tadi, E. Lehtonen, T. Hurnanen, J. Koskinen, J. Eriksson, M. Pänkäälä, M. Teräs, T. Koivisto, A real-time approach for heart rate monitoring using a

Hilbert transform in seismocardiograms, Physiol. Meas. 37 (11) (2016) 1885–1909.
[26] D.M. Salerno, J.M. Zanetti, L.A. Green, M.R. Mooney, J.D. Madison, R.A. Van Tassel, Seismocardiographic changes associated with obstruction of coronary blood flow during balloon angiography, Amer. J. Cardiol. 68 (2) (1991) 201–207.
[27] R.A. Wilson, V.S. Bamrah, J. Lindsay Jr., M. Schwaiger, J. Morganroth, Diagnostic accuracy of seismocardiography compared with electrocardiography for the anatomic and physiologic diagnosis of coronary artery disease during exercise testing, Amer. J. Cardiol. 71 (7) (1993) 536–545.
[28] C.A. Wick, J.J. Su, J.H. McClellan, O. Brand, P.T. Bhatti, A.L. Buice, A.E. Stillman, X. Tang, S. Tridandapani, A system for seismocardiography-based identification of quiescent heart phase: implications for cardiac imaging, IEEE Trans. Inf. Technol. Biomed. 16 (5) (2012) 869–877.
[29] M. Becker, A.B. Roehl, U. Siekmann, A. Koch, M. de la Fuente, R. Roissant, K. Radermacher, N. Marx, M. Hein, Simplified detection of myocardial ischemia by seismocardiography, Herz 39 (5) (2014) 586–592.
[30] A.K. Verma, R. Fazel-Rezai, J.M. Zanetti, K. Tavakolian, Preliminary results for estimating pulse transit time using seismocardiogram, Am. J. Respir. Med. 9 (2) (2015), 020916.
[31] P.K. Jain, A.K. Tiwari, V.S. Chourasia, Performance analysis of seismocardiography for heart sound signal recording in noisy scenarios, J. Med. Eng. Technol. 40 (3) (2016) 106–118.
[32] T. Hurnanen, E. Lehtonen, M.J. Taxi, T. Kuusela, T. Kiviniemi, A. Saraste, T. Vasankari, J. Airaksinen, T. Koivisto, M. Pänkäälä, Automated detection of atrial fibrillation based on time-frequency analysis of seismocardiograms, IEEE J. Biomed. Health Inform. 21 (5) (2017) 1233–1241.
[33] W.Y. Lin, W.C. Chou, P.C. Chang, C.C. Chou, M.S. Wen, M.Y. Ho, W.C. Lee, M.J. Hsieh, C.C. Lin, T.H. Tsai, M.Y. Lee, Identification of location specific feature points in a cardiac cycle using a novel seismocardiogram spectrum system, IEEE J. Biomed. Health Inform. 22 (2) (2018) 442–449.
[34] S. Kay, The effect of noise on the autoregressive spectral estimator, IEEE Trans. Acoust. Speech Signal Process. 27 (1979) 478–485.
[35] H. Akaike, A new look at the statistical model identification, IEEE Trans. Autom. Control 19 (1974) 716–723.
[36] M. Unser, A. Aldroubi, A review of wavelets in biomedical applications, Proc. IEEE 84 (4) (1996) 626–638.
[37] I.R. Pouymiro, E.V. Cordova, F.E.V. Parez, Robust detection of AO and IM points in the seismocardiogram using CWT, IEEE Latin Amer. Trans. 14 (11) (2016) 4468–4473.
[38] R.A. Fisher, Intraclass correlations and the analysis of variance, in: Statistical Methods for Research Workers, Oliver and Boyd, Edinburgh, Scotland, 1954, Available online: http://psychclassics.yorku.ca/Fisher/Methods/.
[39] K.O. McGraw, S.P. Wong, Forming inferences about some intraclass correlation coefficients, Psychol. Methods 1 (1) (1996) 30–46.
[40] J.M. Bland, D.G. Altman, Statistical methods for assessing agreement between two methods of clinical measurement, Lancet 327 (8476) (1986) 307–310.
[41] S.G. Mallat, A theory for multiresolution signal decomposition: the wavelet representation, IEEE Trans. Pattern Anal. Machine Intell. 11 (7) (1989) 674–693.
[42] I. Daubechies, Orthonormal bases of compactly supported wavelets, in: Ten Lectures on Wavelets, SIAM, Pennsylvania, USA, 1992.
[43] S. Mallat, Translation-invariant dyadic wavelet transform, in: A Wavelet Tour of Signal Processing: The Sparse Way, 3rd ed., Academic Press, Burlington, USA, 2009.
[44] A. Rodríguez-Molinero, L. Narvaiza, J. Ruiz, C. Gálvez-Barrón, Normal respiratory rate and peripheral blood oxygen saturation in the elderly population, J. Amer. Geriatr. Soc. 61 (12) (2013) 2238–2240.
[45] A.A. Sarkady, R.R. Clark, R. Williams, Computer analysis techniques for phonocardiogram diagnosis, Comput. Biomed. Res. 9 (1976) 349–363.
[46] C. Torrence, G.P. Compo, A practical guide to wavelet analysis, Bull. Amer. Meteor. Soc. 79 (1) (1998) 61–78.
[47] S.L. Marple Jr., Multichannel spectral estimation, in: Digital Spectral Analysis With Applications, Prentice Hall, New Jersey, USA, 1987.
[48] A.V. Oppenheim, R.W. Schafer, J.R. Buck, The discrete fourier transform, in: Discrete-Time Signal Processing, 2nd ed., Prentice Hall, New Jersey, USA, 1999.
[49] MATLAB code for intraclass correlation coefficient, by A. Salarian. Available online: https://www.mathworks.com/matlabcentral/fileexchange/22099-intraclass-correlation-coefficient-icc.
[50] T.K. Koo, M.Y. Li, A guideline of selecting and reporting intraclass correlation coefficients for reliable research, J. Chiropr. Med. 15 (2) (2016) 155–163.
[51] ANSI/AAMI EC13, Cardiac Monitors, Heart Rate Meters, and Alarms, Association for the Advancement of Medical Instrumentation, 2002.
[52] Instructions for Use, IntelliVue Patient Monitor, MP20/30, MP40/ 50, MP60/70/80/90, Philips.